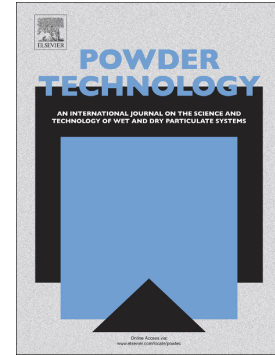| Title	Multiscale digital twin for particle breakage in milling: From nanoindentation to population balance model
Authors	Wang, Li Ge;Ge, Ruihuan;Chen, Xizhong;Zhou, Rongxin;Chen, Han-Mei
Publication date	2021-03-06
Original Citation	Wang, L. G., Ge, R., Chen, X., Zhou, R. and Chen, H.-M. (2021) 'Multiscale digital twin for particle breakage in milling: From nanoindentation to population balance model', Powder Technology, 386, pp. 247-261. doi: 10.1016/j.powtec.2021.03.005
Type of publication	Article (peer-reviewed)
Link to publisher's version	10.1016/j.powtec.2021.03.005
Rights	
Download date	2024-05-06 23:34:58
Item downloaded from	https://hdl.handle.net/10468/11240

Journal Pre-proof

Multiscale digital twin for particle breakage in milling: From nanoindentation to population balance model

Li Ge Wang, Ruihuan Ge, Xizhong Chen, Rongxin Zhou, Han-Mei Chen

Please cite this article as: L.G. Wang, R. Ge, X. Chen, et al., Multiscale digital twin for particle breakage in milling: From nanoindentation to population balance model, *Powder Technology* (2021), https://doi.org/10.1016/j.powtec.2021.03.005

Multiscale Digital Twin for Particle Breakage in Milling: From Nanoindentation to Population Balance Model

Li Ge Wang[a,b], Ruihuan Ge[b], Xizhong Chen[c,d]*, Rongxin Zhou[e], Han-Mei Chen[f]

[a]Process Systems Enterprise, Hammersmith, London, UK

[b]Department of Chemical and Biological Engineering, University of Sheffield, UK

[c]Process and Chemical Engineering, School of Engineering, University College Cork, Ireland

[d]Department of Materials Science & Metallurgy, University of Cambridge, UK

[e]Wolfson School of Mechanical, Electrical and Manufacturing Engineering, Loughborough University, UK

[f]School of Architecture, University of Liverpool, UK

*Email : Xizhong.Chen@ucc.ie

Abstract

A multiscale modelling approach to integrate resultful information of particle breakage at distinct scales is presented for quantitative prediction of a milling process. The nanoindentation test of zeolite particles is carried out to provide the deterministic value of mechanical properties, prior to which the Hertz based contact theory is described. The impact pin milling test is made to measure the particle size distribution subject to three rotary speeds. The population balance model composed of selection function and breakage function is developed to predict the varying milling operations based on successful model validation. With the hybrid of theoretical, experimental and numerical avenues, a conceptual multiscale modelling roadmap with complementary strength is proposed. The best available information spanning distinct scales are scoped where the interaction of physical twin and digital twin is highlighted. Global system analysis of the key parameters provides projected confidence in milling performance beyond the existing experimental space.

Keywords: Multiscale milling; Digital twin; Particle breakage; Nanoindentation; Population balance model; Model Validation

Nomenclature

a	Fitting parameter, -
A	Contact area, m^2
b	Fitting parameter, -
B	Milling matrix, -
B_M	Breakage function, -
$B(v,t)$	Birth rate, m^{-3}s^{-1}
B_{break}	Birth rate of breakage, m^{-3}s^{-1}
c	Fitting parameter, -
d	Particle diameter, m
D_{break}	Death rate of breakage, m^{-3}s^{-1}
E	Elastic modulus, MPa
f	Feed particle size distribution, -
f_{Mat}	Material dependent parameter, -
f_{Mat}^*	Evolved version of material dependent parameter, -
F_{in}	Particle flow rate, kg/h
h	Indent depth, m
H	Hardness, MPa
k	Impact number, -
K_c	Fracture toughness, Pa m$^{0.5}$

l	Crack length, m
m	Fitting parameter, -
m_i	Particle mass, g
M_m	Mother particles mass, g
M_{de}	Debris particle mass, g
n	Population density of length function, m^{-3}
N	Number of breakage events, -
p	Output size distribution, -
P	Load, N
P_x	Breakage probability of particle size x, -
q	Fitting power exponent, -
R	Particle radius, min
S	Stiffness, N m^{-1}
S_i	Selection function, -
t	Time, s
w_i	Mass fraction, -
$W_{m,kin}$	Mass specific impact kinetic energy, J kg^{-1}
$W_{m,min}$	Threshold kinetic energy, J kg^{-1}
W_v	Volumetric specific stressing energy, J kg^{-1}
x	Initial particle size, mm

y Fragment size, mm

y' Minimal particle size, mm

z Fitting parameter, -

Greek symbols

α Fiting parameter, -

β_{max} Crack extension energy per unit of resulting surface, J m^{-2}

ρ Density, kg m^{-3}

σ Strength, MPa

τ Residence time, s

ν Poisson's ratio, -

ψ Shape parameter, -

1 Introduction

Particulate system is widely recognized to be in a multiscale nature and efforts in multiscale modelling of particulate system are devoted to creating flexible and efficient models by linking two or more partial models spanning at different spatial and temporal scales [1]. As a common unit operation of particulate materials across many industries, milling is intended for desired particle size reduction to achieve well-defined product quality. Meantime, scientific understanding of milling process covers many length scales from the molecular level at the focal point of a crack to the process level of milling circuit including feeders, mills and classifiers [2]. The molecular dynamics simulation of nanoindentation on the particle surface was carried out to study the influence of indentation contact, deformation, and adhesion on multi-layered films [3]. The experimental difficulty of maintaining minute depth penetration can be readily solved by molecular dynamics (MD), which effectively captures the initial crack, identify the microscopic mechanism and offer mechanical insights

into the microscopic behaviour [3]. Due to the similarities amongst fracture, friction and adhesion on a molecular level, these three mechanical behaviours can be distinguished by the magnitude and direction of acting forces. Other examples of nanoindentation fracture based on molecular dynamics simulation can be found elsewhere [4,5]. The significance of molecular dynamics simulation is to understand the dynamic material behaviour in the vicinity of a single crack, which is foundational to the cracking process of a particle but otherwise is almost impossible solely by experimentation [2,3].

Particle scale of breakage mechanics is usually achieved by imposing stressing conditions on individual particles. The compressive loading of particle breakage can be carried out to measure the characteristic strengths such as crushing force, breakage energy and breakage stress. The reason behind the compressive strength measurement is because every particle undergoing the stressing conditions such as collision, attrition, disintegration and fragment is associated with its mechanical stress. The evaluation of compressive strength for a great variety of particulate materials was performed by many researchers [6–8]. Furthermore, the compressive loading curve can also be used to evaluate the failure mode of particles, i.e. elastic deformation, brittle deformation and ductile deformation [9]. Besides the compressive loading mode, the impact loading of particle breakage mechanics has also been widely studied from the lab scale in the literature. The effects of impact velocity, impact angle, impact orientation, impact threshold were mainly studied to assess the breakage propensity and product size distribution after impact loading. The reason for performing the single particle impact breakage is because of its similarity of stressing conditions, which are physically identical to that in the comminution [10]. As a result, considerable efforts have been devoted to developing the impact testing systems and quantitative breakage models to predict the particle breakage probability and product size distribution as a function of the stressing conditions such as the impact velocity, impact number and impact angle.

Alternatively, miniaturized milling devices in the lab scale were developed to allow for the determination of material properties associated with the breakage models in a more practical and less time consuming method compared to single particle impact tests [11]. Furthermore, the database from the lab scale milling tests provides benchmark values of product size distribution for computational model validation. Vogel and Peukert [12] developed a multiscale modelling of particle breakage from single particle impact to

modelling of impact mills. It was assumed that the milling process is composed of machine and material functions. The machine function is made up of milling types and operating conditions. The material function includes the breakage probability and product size distribution which can be further related to the operational conditions in the machine function. Despite good agreement in the experimental results and the simulations by population balance model, the mechanical insights to correlate the material functions are unavailable in their study.

This paper aims to present a mechanistic-based multiscale modelling approach for particle breakage through interlinking the best available information at each scale for achieving a predictive digital twin for milling processes. The multiscale approach starts from the nanoindentation of zeolite particles to measure the mechanical properties of hardness and fracture toughness. The mechanical response of zeolite particles subject to indentation also provides the theoretical basis to liken the breakage pattern of impact loading in the particle scale. The experimental breakage tests are carried out in the process scale of an impact pin mill, which serves to provide quantitative dataset for model validation. A multiscale modelling roadmap to study particle breakage in milling is proposed to integrate the complementary strength across different scales and eventually form a predictive capacity of the product quality. As the digital design and operation of particulate processing is playing a significant role in the era of Industry 4.0, the concept of Digital Twin is reflected in the multiscale modelling roadmap of a milling process. The population balance model is properly validated with the experimental data and further extended to explore virtual design space by the global system analysis. The multiscale modelling of particle breakage in the present study provides alternative means of model driven design for a milling process through a hybrid of theoretical, experimental and numerical methods.

2 From theory to characterisation: Nanoindentation

2.1 Nanoindentation Mechanism

Instrumented nanoindentation of probing mechanical properties such as hardness and elastic modulus has emerged as an important technique to elaborate the mechanical behaviour on a small length scale [13]. The attractiveness of nanoindentation stems from its readiness to determine the key mechanical properties from the stress-strain curve without

imaging the hardness impression [13]. Most importantly, the mechanical response observed from nanoindentation underpins the foundation to develop particle breakage models subject to impact loading due to the likeness between indentation fracture and impact breakage [14,15]. It has been shown that the loading and unloading curve may be approximated by the power law relation:

$$P = \alpha h^m$$

$$P = \alpha (h - h_f)^m \qquad \text{(1a)}$$

(1b)

where α and m are power fitting constants. Values of constants observed should be consulted for further details by Oliver and Pharr [13,16].

Figure 1 Schematic of indentation load-displacement data (Modified from Wang et al. [17])

Differentiation of Eq. 1b with respect to $(h - h_f)$ gives the contact stiffness,

$$S = \frac{dP}{d(h-h_f)} \qquad \text{(2)}$$

Figure 2 shows a cross section of indentation with parameters used in the analysis. The total displacement h is given by

$$h = h_c + h_s \qquad \text{(3)}$$

where h_c is the vertical distance by penetration of indenter and h_s is the vertical displacement of surface at the perimeter of the contact. In Figure 2, a is the contact radius between the indenter and the specimen surface. Φ is the half-included angle of the indenter, which depends on the indenter geometry- $\Phi = 70.3^o$ for Berkovich indenter.

Figure 2 Schematic illustration of indentation with parameters characterizing the contact geometry (Modified from Oliver and Pharr, 1992 [16])

The contact area, A, can be expressed as a function of the plastic depth h_c

$$A = k h_c^2 \qquad \text{(4)}$$

For Berkovich and Vickers indenters, the shape factor k is 24.5.

Once the contact area is determined, the hardness of a material is given.

$$H = \frac{P_{max}}{A} \tag{5}$$

where P_{max} is the maximum load applied to the sample during indentation loading and A is the corresponding contact area of P_{max}.

The unloading stiffness S can be related to contact area A and effective elastic modulus E_{eff}

$$S = \frac{2}{\sqrt{\pi}} E_{eff} \sqrt{A} \tag{6}$$

The effective elastic modulus E_{eff} is related to the Young's modulus and Poisson's ratio of the sample and the indenter. It is defined by

$$\frac{1}{E_{eff}} = \frac{1-v_s^2}{E_s} + \frac{1-v_i^2}{E_i} \tag{7}$$

where subscripts s and i denote the sample and indenter, respectively.

The effective elastic modulus considers the fact that elastic displacement occurs in both the indenter and the sample. The Young's modulus of the sample can thus be determined with the known value of Young's modulus and Poisson's ratio for the indenter and the estimated value of Poisson's value for the sample.

Fracture toughness represents the ability of material to resist brittle fracture when a crack is present. A basic equation for evaluating the fracture toughness (K_c) of material is given [18]

$$K_c = 0.0143 \left(\frac{E}{H}\right)^{\frac{2}{3}} \left(\frac{c}{l}\right)^{1/2} \left(\frac{P_{max}}{c^{3/2}}\right) \tag{8}$$

where P_{max} is the maximum applied load, E and H are the Young's modulus and hardness of the sample, respectively. c is the length from the center of the indent to the tips of the radial cracks. α is an empirical constant dependent on the indenter geometry. For the Berkovich and Vickers indenter $\alpha = 0.016$. Figure 3 illustrates the schematic diagram of crack failure modes under Vickers indentation.

Figure 3 shows that radial cracks extend outward from the boundary of indentation along the sample surface and sub lateral cracks initiate below the indentation centre and extend upward to the sample surface. It should be noted that the crack length is strongly

dependent on the local microstructure and several radial cracks need to be measured for statistical reliability.

Figure 3 Schematic illustration of crack failure modes and dimensions for Vickers indentation (Modified from Anstis et al.[18])

2.2   Measurement method

The NanoTest nanoindenter in Figure 4 is equipped with a video microscope for accurate positioning of the indenter and is capable of producing well-defined load-displacement curve. A diamond three-sided Berkovich indenter is mounted to a pendulum which can move freely by a frictionless pivot. The Berkovich indenter is imposed close to the particle by flowing an electric current through the wire coil. The value of loading force depends on the amount of current through the coil. The corresponding displacement is recorded by the variation of voltage from capacitance plates. The sample holder is used to align the indenter using three direct current motors with a XYZ micro-positioner mounted. Considering the material structure or reactions with oxygen in the air, the penetration depth of indentation is typically influential on the resulting value of hardness and Young's modulus [19]. A preliminary set of indents up to maximum indentation load was carried out for each sample.

Figure 4 Schematic of Nanoindentation tester (Modified from Taylor et al. 2004 [20])

The particle was attached to the nanoindenter by means of microscope where the central indent was placed. The focused region was considered to be the center of the particle on the indentation plane because of the high sphericity of the particle and the narrow field depth of the microscope. The initial maximum load was applied to 50 mN at a loading rate of 2 mN/s at the first stage of the preliminary test. Then the applied load was reduced to 30% of the preceding maximum load at the same loading/unloading rate, prior to reloading to a maximum load greater than the last maximum. This measuring procedure was repeated until a maximum load of 500 mN was achieved before the full unloading of the sample. To have a statistical reliable value of hardness and Young's modulus, 10 zeolite particles are indented using the Nanoindentation tester. In Figure 5 for each particle, a matrix of 3 rows

by 3 columns is used with a separation distance of 80 μm between each grid indent to avoid interactive influence from the neighbouring indent points. The reason for indenting multiple girds is in recognition of heterogeneity of particle surface at the nanoscale. Compared to the literature distance, 80 um is deemed sufficiently large to avoid neighbouring interaction [20].

Figure 5 Schematic of indentation on zeolite particle surface by 3x3 matrix grid point (a) 3D view and (b) top view.

2.3   Property measurement

2.3.1   Hardness

For each of ten indents, the Young's modulus obtained through Eqs. 6 and 7 assuming the Poisson ratio of both materials to be 0.25. The hardness is measured using Eqs. 4 and 5. By so doing, the value of hardness and Young's modulus can be determined from the multiple loadings of 1.4-1.7 mm zeolite. Figure 6 shows that the hardness of zeolite particle (1.4-1.7 mm) is varied from 0.11 GPa to 0.147 GPa with the Young's modulus ranging from 5.18 GPa to 5.94 GPa. The hardness of the zeolite particle increases with the increase of maximum load from 50 mN to 200 mN, beyond this range the value of hardness is levelled off until 500 mN.

Figure 6 Variation of zeolite (1.4-1.7 mm) mechanical properties with indent load

The Young's modulus exhibits a slight increase as maximum indentation load is increased until a maximum load of 100 mN. Beyond this range, there is a slight reduction in Young's modulus. Considering the slight variation of Young's modulus and hardness beyond a maximum indentation load of 200 mN, the maximum load of 200 mN was adopted for the subsequent measurements of Young's modulus and hardness. To select an appropriate measurement loading, a compromise should be made between sufficient indentation depth to overcome surface roughness and shallow enough depth to measure contact-relevant properties. In the case of low loading force, it presents a challenge to maintain a reasonably good contact with the particle surface, generating potential noisy load-displacement plots which are hard to analyse [21]. Meantime, the indentation depth and area may not be large

enough to be visibly measured by microscopy. Other factors influencing the property measurement include slipping and friction between tip and particle [22].

These aforementioned influences can be mitigated by increasing the loading force where the values of hardness and Young's modulus can stabilize [22]. However, in case of increasingly high loading force, severe cracking is very likely to occur, leading to a difficulty in accurately measuring the contact area and thus misleading results of hardness and Young's modulus. Consideration of all these factors leads to a decision of choosing 200 mN for zeolite particle indentation herein. To keep consistence of contact area and unloading stiffness, the Young's modulus is measured as the same loading force for hardness. However, it should be noted that the selection of loading force is material dependent and 200 mN is only limited to zeolite particles in this work.

Following the maximum load of 200 mN for each indentation on the same particle, the load-displacement curve for a single particle of 1.4-1.7mm zeolite with total nine indentations is shown in Figure 6. It can be observed that in Figure 7 the indent number 7 is anomalous with an incredibly large penetration as compared to other indents. Such incident may be accounted by premature detection of a very small force increase prior to the penetration of the true sample surface (e.g. by contacting dust; loose material adhered to the surface, or the tip of a highly rough area). This gives rise to artificially low values of hardness and Young's modulus due to the overestimate of penetration depth and thereby plastic area. Although the nanoindentation has been widely used for mechanical property measurement, little work has been done in optimizing this method with a unified principle for loading prescription, indentation depth as well as the separation distance of grid especially for heterogeneous materials [5]. One principle in a careful selection of indentation depth is sourced in the literature and it is found that the ratio of h/D < ~0.1 will give rise to a statistically independent value of hardness and Young's modulus. h denotes the indentation depth and D denotes characteristic size of heterogeneity factor, e.g. separation distance. In this work, the ratio of h/D is set as 0.11 leading to a threshold value of 8800 nm maximum depth given the separation distance 80 μm.

In view of this, such incidents in zeolite particles as observed in Figure 7 (Indents Number 6 and 7) are not taken into account in this work. The data of average Young's modulus and hardness for the 1.4-1.7 mm zeolite particles is tabulated in Table 1, including all the indents

on a given particle. The variation in the values of Young's modulus and hardness is expected due to the abovementioned heterogeneity. Likewise, the variation of mechanical properties such as Young's modulus is also found in the compression loading test. More details regarding the alternative way of measuring Young's modulus can be found in our recent work [17].

Figure 7 Force-displacement for 9 indents on a single 1.4-1.7 mm zeolite

2.3.2   Fracture toughness

Fracture toughness was measured by the synergic action of microindentation and SEM. Initially, 40 particles of each material and size class were indented by the prescribed load (5 N for zeolite). Figures 8 shows examples of generated cracks in zeolite particles at 1.4–1.7 mm and 2.0-2.36 mm respectively. The values of α, t, c and the resulting K_c are evaluated and reported in IFPRI final report [23,24]. The statistics of measured fracture toughness for zeolite particles is summarized in Table 2. A number of studies to predict the breakage propensity of particles using mechanical properties have been highlighted in the work of Taylor et al. [20,21]. It was found that the ratio of hardness to fracture toughness, i.e. brittleness provides better discrimination in breakage patterns. The correlation of brittleness with the key input parameters in the numerical method will form an attempt in the following section of this work.

Figure 8 Cracks generated in a zeolite particle for fracture toughness measurement

3   Experimental avenue: Impact Pin Mill

This section presents the experimental avenue to decipher the breakage mechanism in the process scale of impact pin mills. It is intended to provide the dataset of ground particle size distribution subject to varying rotary speeds. The feature of this section is to provide a relatively small volume of dataset for multiscale model validation and eventually to substantially reduce the amount of experimental trials where the power of model-based system engineering will be unleashed. The intrinsic interlink between the nanoscale and

process scale of particle breakage is laid on the fact that the fracture toughness has been shown to strongly associated with milling [21,25].

3.1 Mill setup and measurement

The tested particles are still chosen as zeolite to keep consistency in a multiscale approach. The milling of zeolite particles is carried out in an impact pin mill, where the detailed configuration is stated in Wang [24]. The objective of this measurement is provision of particle size distribution of milled zeolite to implement the model validation.

The particle size produced from the impact pin mill is determined by numerous factors such as configuration of pins, mechanical properties of the fed particles, the rotary speed, and the feed rate. The advantage of impact pin mill is the smaller fineness of milled particle compared to the hammer mill and less occupied floor space. A distinct disadvantage of the impact pin mill is the high wear rate and heat generation due to friction.

The configuration of impact pin mill is shown in Figure 9, which includes the stationary and rotary plates. In each plate, there are four levels of pins equipped where the number of pins increases with the layer radius. The precise configuration of the pin information is summarized in Table 3. The rotary plate of pin layer is named with prefix R whilst the stationary plate of pin layer is named with prefix S.

Figure 9 Configuration of impact pin mill UPZ 100 (Modified from Wang, 2016 [24])

The zeolite particles with initial size 1.2-2.0 mm are fed to the mill by vibrational feeder on the top and enter the milling zone centrally. Accelerated by centrifugal forces, the particles spin outwards and are stressed by the rotary disc. In the present study of milling experiment, the rotary speed is varied with the values of 8000 RPM, 10000 RPM and 12000 RPM. The feed rate is fixed at 19 kg/h for the total feed mass of 500 g zeolite particles. After the particles pass through the interacting pin discs, they are transported vertically downwards to the collecting pan. The particle size distribution of the milled product is determined by Mastersizer 2000.

3.2 Particle size distribution

Figure 10 presents the particle size distribution of milled zeolite subject to three rotary speeds, i.e. 8000 RPM, 10000 RPM and 12000 RPM. It indicates that the product size is significantly reduced following a clear shift to the left side compared to the initial feed size. This dramatic size reduction is echoed with the selection of Vogel and Peukert model where fragmentation is the dominant mechanism subject to the high rotary speed. The milled product size is ranged from 1 μm to around 300 μm and the d_{50} is way below 100 μm, which falls in line with the milling capacity of UPZ 100. In terms of the rotary speed, it can be seen that finer product size is produced with increased rotary speed. It is interesting to note that the finest particle size to be ground is approximately 1 μm. The unbroken size below 1 μm is speculated with the intrinsic component of zeolite and implies a lower boundary value which can be defined as a threshold value for particles to break.

Figure 10 Cumulative particle size distribution for zeolite (1.2-2.0 mm) under three rotary speeds in the impact pin mill

For clarity, the PSD quantiles, i.e. d_{10}, $d_{.0}$, d_{50}, d_{75}, and d_{90} of zeolite particles are summarized in Table 4. A series of grindability indexes (i.e. size reduction ratio, size span and grinding energy consumption) as a function of these PSD quantiles can be attempted to further interpret the fineness of milling size reduction. However, the grindability assessment are not attempted in the present study, which is beyond the scope of this paper. Instead, the reason for listing these PSD quantiles is to provide the dataset for the population balance model calibration and validation and thus establish the predictive capacity for milling process.

4   Numerical avenue: Population Balance Model

The population balance model (PBM) has been widely used in a great variety of particulate processing operations to track the particle attributes evolution at the process scale [26,27]. The general form of PBM for a batch mill can be given as:

$$\frac{dm_i(t)}{dt} = -S_i m_i(t) + \sum_{j=1}^{i-1} b_{i,j} S_j m_j(t) \tag{9}$$

where $m_i(t)$ denotes the mass of particle in the ith size interval at milling time t; S_i and $b_{i,j}$ denote the selection function and the breakage function respectively. The selection function, S_i is the specific breakage rate describing the fraction of particles in the size fraction i from time t to $t + dt$. The selection function S_i can be expressed as $S_i = S_x * P_x$. S_x is the breakage rate and P_x is the breakage probability. $b_{i,j}$ is used to describe the breakage distribution function of particles between the size interval i and j. As seen in Eq. (9), to predict the size reduction from a batch milling process, a prior knowledge of S_i and $b_{i,j}$ has to be known. There are numerous approaches to determine the parameters residing in the selection function and breakage function. A commonly used method is to fit the model parameters from single particle impact data and then to scale up the function parameters in PBM [28]. Alternatively, direct back-analysis of population balance model based on the process scale of milling data is employed where the back-calculated parameters are searched by the minimum of the sum of squared errors (SSEs). The advantage of back-analysis method is that there is no need to perform single impact breakage of particles as the experimental and numerical data are only constrained in the process level. On the other hand, the drawback of this method is also manifest that the mechanistic interdependency of the input parameters in PBM are lacking without the precise information from the smaller scales. As a consequence, prior to the parameter estimation in the PBM, a critical aspect is to choose the appropriate selection function and breakage function corresponding to the dominant stressing conditions in the targeted milling process. Most importantly, the deterministic relationship from multiscale scales can be found to provide quantitative information for the input parameters in PBM. In view of this, the detailed form of the selection function and breakage function is presented as below for the purpose of impact pin mill where the high impact velocity and impact frequency are prevailing [29,30].

In terms of the average residence time τ in the impact pin mill, it is calculated by dividing the particle mass m in the mill volume V by the particle flow rate F_{in}, which gives:

$$\tau = \frac{m}{F_{in}} \quad (10)$$

The flow rate of zeolite particles in this study is 19 kg/h.

4.1   Selection function

There are many types of selection function developed to describe the breakage rate of particulate materials subject to impact loading circumstances. In this study, the selection function of Vogel and Peukert model is adopted due to its numerous superiority such as consideration of impact velocity, impact number, threshold impact energy and particle size material dependent parameters which can be linked with the mechanical properties measured from nano-scale.

The Rumpf theory [31] summarized the influential parameters on the particle breakage leading to the following equation:

$$P_x = f\left(k, \frac{W_v x}{\beta_{max}}, \frac{E' l_i}{\beta_{max}}, \frac{H}{E'}, \frac{E''}{E'}, \frac{l_i}{x}, \frac{v_d}{v_{el}}, \frac{v_{fract} x}{v_{el}}, \psi, \nu\right) \quad (11)$$

where P_x is breakage probability; k denotes the frequency of stressing events, W_v is the volumetric specific stressing energy, β_{max} is the crack extension energy per unit of resulting surface, E' and E'' represent the storage and viscous loss modulus of the particulate material, l_i denotes the inherent pre-existing crack length, H and x denote the hardness and initial particle size respectively, ψ and ν are the shape parameter and Poisson ratio of the particles; v_{fract} and v_{el} are the velocity of crack propagation and the velocity of propagation of elastic waves.

Eq. (11) takes into account all the potential parameters relevant to particle breakage and it can be simplified in the case of impact conditions. For example, the velocity of propagating cracks, v_{fract} is usually dramatically lower than the velocity of elastic waves, v_{el} for brittle materials alike [12]. Moreover, the ratio between l_i and x is found less influential on the comminution results for the coarse materials. Simplifying Eq. (11) gives rise to:

$$P_x = f\left(k, \frac{W_v x}{\beta_{max}}, \frac{E' l_i}{\beta_{max}}, \frac{H}{E'}, \frac{E''}{E'}, \psi, \nu\right) \quad (12)$$

From the perspective of fracture mechanistic model, Weichert theory [32] presented the Weibull statistics for the application of comminution. The probability function as proposed by Weichert gives:

$$P_x = 1 - \exp(-z(\frac{\sigma}{\sigma_s})^m) \quad (13)$$

where σ and σ_s denote the applied strength and reference strength whilst z and m are the fitting parameters. Note that a detailed description of Weichert model can be found in

Vogel and Peukert [12], which leads to the expansion of Eq. (13) as a function of Hertz theory [33].

The Vogel and Peuket model was developed on the basis of Rumpf's similarity theory and Weibull statistics of fracture mechanics and it gives [34]:

$$P_x = 1 - exp\{-f_{Mat}xk(W_{m,kin} - W_{m,min})\} (14)$$

where P_x is breakage probability; $W_{m,kin}$(J/kg) is mass-specific kinetic energy; x and k are particle size and impact number. f_{Mat} and $W_{m,min}$ are the material dependent properties.

Amongst the parameters in Vogel and Peukert model, the parameter f_{Mat}, characterising the resistance of particles against fracture in impact comminution and the minimum specific energy $W_{m,min}$ are the two parameters which embody the mechanistic properties and particle intrinsic property. Specifically, the minimum specific energy $W_{m,min}$ is usually lumped as $x * W_{m,min} = constant$ where the particle property of size effect can be reflected [35]. In other words, the minimum specific energy increases as the particle size is reduced.

In light of the significance of these two parameters f_{Mat} and $W_{m,min}$, the single particle impact tests are usually performed to measure the deterministic value of f_{Mat} and $W_{m,min}$. The employment of single particle impact tests has been well-trodden and many examples of this method can be found in the literature [12,28,35,36]. Despite the success of single particle impact tests, the drawback of this method is the missing linkage of any mechanical properties associated with f_{Mat} and $W_{m,min}$. As the main thrust of the present study is to establish a multiscale mechanistic interdependency for particle breakage, it is critically important to set up the mechanistic linkage associated with Vogel and Peukert model. Meier et al. [22] made the first attempt to correlate the material dependent parameters f_{Mat} and $x * W_{m,min}$ with the intrinsic mechanical properties measured from nanoindentation. The adjusted parameter f_{Mat}^* can be expressed when the particle is impacted on a target with Young modulus E_{target}:

$$f_{Mat}^* = c_1\rho \left(\frac{H}{K_c}\right)^{2.5}$$

$$f_{Mat}^* = f_{Mat}\left(1 + \frac{E}{E_{target}}\right) \quad (15a)$$

(15b)

c_1 is a proportionality constant and ρ is the particle density. When the target Young's modulus is much higher than the particle, the adjusted parameter f_{Mat}^* can be approximated as f_{Mat}. f_{Mat}^* in Eq. 15a is the evolution of f_{Mat} when the impact target property E_{target} is considered. Eq. 15a shows the mechanistic relationship from nanoindentation to particle impact breakage. Eq. 15b gives the relationship between f_{Mat}^* and f_{Mat}. When the impact target E_{target} is way beyond the particle modulus, f_{Mat}^* retreats to the same value of f_{Mat}. Details of derivation of f_{Mat}^* are described from the original source by Meier et al. [22]. Note that $\frac{H}{K_c}$ is a widely used term, i.e. brittleness to describe the milling behaviour such as the transition from brittle to ductile deformation.

A simple way to fit the proportionality constant c_1 is to reform Eq. (15a), which gives:

$$\ln\left(\frac{f_{Mat}^*}{\rho}\right) = lnc_1 + 2.5 * (lnH - lnK_c) \quad (16)$$

Given a deterministic value of f_{Mat}^*, another material dependent property $x * W_{m,min}^*$ gives:

$$x * W_{m,min}^* = c_2 \frac{1}{\rho}\left(\frac{f_{Mat}^*}{\rho}\right)^{-1.5}$$

$$x * W_{m,min}^* = x * W_{m,min}\left(1 + \frac{E}{E_{target}}\right)^{-1} \quad (17a)$$

(17b)

where c_2 is a proportionality constant in Eq. (17).

The determination of $x * W_{m,min}$ is found to be increasingly inaccurate for small values of the energy threshold and exhibits larger scatter than f_{Mat} from milling experiments [22]. In practice, Eqs. 15b and 17b can retreat to Eqs. 15a and 17a.

Rearrangement of Eq. (17a) for simpler expression between $x * W_{m,min}^*$ and f_{Mat}^* and it gives:

$$f_{Mat}^* = a * (x * W_{m,\min}^*)^b$$
$$(18)$$

where a is a lumped effect of c_2 and ρ, of which the given value is 0.22 by Lecoq et al. [37]; b is the fitting constant -0.67 as derived from Eq. (17) with another close value reported as -

0.63 from Lecoq et al. [37]. Eq. (18) is used to show the dependence between f^*_{Mat} and $x * W^*_{m,min}$. In contrast, Eqs. 15 and 17 are intended to show the relationship between nanoindentation and key parameters in the particle scale from Vogel and Peukert model [34].

4.2 Breakage function

Analogue to the selection function, many forms of breakage functions are also developed to describe the particle size distribution after impact events. Despite a great wealth of their forms, the principle of breakage function can be schematically depicted in Figure 11.

Figure 11 Schematic illustration of size grade in breakage function (Modified from Lyu et al. [38])

Assuming division of 5 size intervals for the ground materials, the cumulative size distribution of ground materials is shown as a function of five classes x_1, x_2, x_3, x_4 and x_5. In milling, it is conventional to number the size intervals from the largest size to smallest size [26]. Hence, x_1 represents the mass fraction in the largest size.

The milled particle size can be divided into n grade and $b_{i,j}$ is usually used to describe the proportion of material falling into grade j from grade i, the mass fraction $b_{i,j}$ can then expressed as:

$$b_{i,j} = B_{i,j} - B_{i+1,j} \tag{19}$$

Given the mill product by p and the feed rate by f, the particles breaking from the top size x_1 and remaining in the top size grade can be expressed:

$$p_1 = b_{11} * f_1 \tag{20}$$

where b_{11} is the mass proportion remaining on the top size after breakage.

Similarly, the mill product for all the other grades gives by [39]:

$$p_2 = b_{21} * f_1$$

$$p_3 = b_{31} * f_1$$

$$p_4 = b_{41} * f_1$$

$$p_5 = b_{51} * f_1$$

(21)

Whilst Eqs. 20 and 21 are used to describe the mill product entering the downside grades based on the top size grade x_1, the material balance in full matrix form is shown as:

$$\begin{bmatrix} p_1 \\ p_2 \\ p_3 \\ p_4 \\ p_5 \end{bmatrix} = \begin{bmatrix} b_{11} & 0 & 0 & 0 & 0 \\ b_{21} & b_{22} & 0 & 0 & 0 \\ b_{31} & b_{32} & b_{33} & 0 & 0 \\ b_{41} & b_{42} & b_{43} & b_{44} & 0 \\ b_{51} & b_{52} & b_{53} & b_{54} & b_{55} \end{bmatrix} \begin{bmatrix} f_1 \\ f_2 \\ f_3 \\ f_4 \\ f_5 \end{bmatrix}$$ (22)

The matrices can be represented in a simple form:

$$p = B * f$$ (23)

where p describes the output size distribution of mill product; B denotes the milling matrix and f denotes the vector describing the feed particle size distribution.

In an expanded form of B with n division of size grades, it gives:

$$B = \begin{bmatrix} b_{1,1} & 0 & 0 & 0 & 0 \\ b_{2,1} & b_{2,2} & 0 & 0 & 0 \\ b_{3,1} & b_{3,2} & b_{3,3} & 0 & 0 \\ \vdots & \vdots & \vdots & \ddots & \vdots \\ b_{n,1} & b_{n,2} & b_{n,3} & \cdots & b_{n,n} \end{bmatrix}$$

(24)

The feature of Eq. 24 is that the values above the diagonal of B are zero as there cannot be any growth term in any top size grade by breakage. Furthermore, for any column in matrix B, it follows with $\sum_{i=j+1}^{N} b_{i,j} = 1$. More details about the milling circuit matrix in Eqs. 20-24 are referred in [39].

Broadbent and Callcott [40] first introduced the breakage matrix to calculate the size reduction and used a geometric progression of sieve sizes for the feed and product size distribution, resulting in a square breakage matrix [41]. A key criterion in selecting the breakage function is the identification of the breakage mechanism in the milling process.

The breakage function in the present study is proposed by Vogel and Peukert [12] and it gives:

$$B_M = \left(\frac{x}{y}\right)^q \frac{1}{2}\left(1 + \tanh(\frac{y-y'}{y'})\right)$$ (25)

where x denotes the initial particle size; y and y' denotes the fragment size and the minimal particle size expected by milling; q is the fitting power exponent. The reason for choosing Eq. (25) is due to its matching regime in fragmentation and widespread usage in high impact mill.

5   Multiscale Modelling Proposal in Milling

5.1   Integrated Multiscale Modelling Roadmap

The overarching goal in the present study is to interlink multiscale information of particle breakage to form predictive accuracy of CQAs (Critical Quality Attributes) in a milling operation, without exhaustion in any single scale. To enable a practical development and implementation of multiscale modelling avenues, we propose an integrated conceptual roadmap to interlink the milling process by a multiscale approach in Figure 12. This integrated framework consists the potential scales involved in the milling process where both the physical twin and digital twin corresponding to each scale are schematically depicted.

In the process scale, the milling tests are usually carried out to study the particle size evolution subject to the dominant stressing events. The CPPs (Critical Process Parameters) in a milling operation need to be identified and their influence on the CQAs (Critical Quality Attributes) should be investigated. On the other hand, the digital twin of the milling operation is carried out to provide the particle dynamics and upscale particle scale information to inform and develop the dynamic-based breakage kernel in the population balance model. An example of DEM-PBM coupling approach for the prediction of an impact pin mill was presented in our recent publication where the impact velocity and impact frequency from DEM is used to inform the process parameters in the PBM model. Similarly, the application of DEM-PBM coupling method into the ball mill, ribbon mill can be found elsewhere [42–44].

In the lab scale, the single particle impact test is mostly employed to study the breakage pattern and breakage propensity in the stressing events pertinent to milling operation. Whilst a great variety of well-established impact testing rigs was developed, the main thrust of single particle stressing tests is to provide quantitative breakage models in describing the particle breakage probability and broken particle size distribution. Other experimentation in

the lab scale includes miniaturized milling tests to identify the dominant stressing events similar to the process scale of milling tests and further to determine the material properties f_{Mat} and $x * W_{m,min}$ as a function of impact velocity, impact number and feed particle size [11].

In the particle scale, as the morphology and internal structure becomes influential for the mechanical behaviour of individual particles [45], the X-ray microcomputed tomography (μCT) combined with the incremental loading tests is the main resort to enable the clear and distinct visualization of the internal density structure. Due to its high resolution, the progressive failure of particle deformation subject to controlled loading stages can be observed where the crack initiation and propagation provides crucial information on the calibration of DEM (Discrete Element Method) modelling of crushable particle breakage. Despite a rich body of particle deformation studies using X-ray μCT, there remains an inherent gap of the incompatibility of particle structure between the X-ray μCT and the numerical prototype. The emerging technology of additive manufacturing has enabled a bespoke particle internal structure and the difficulty of directly and precisely comparing the particle deformation between experiment and DEM can be readily overcome by 3D printed particles. The method of applying 3D printed particles to calibrate the bonded contact model has been proposed by Ge et al. [46,47]. Using 3D printing, particle clusters with regular and random structures can be readily manufactured for strength testing [48]. Valuable data from the micro-scale single bond parameters to the meso-scale particle clusters is used for bonded contact model calibration [46].

The nanoscale study of particle breakage is carried out to measure the key mechanical attributes such as Young's modulus, hardness and fracture toughness. Most importantly, the indentation fracture mechanics has provided foundational basis into the breakage model development where the cracking patterns provides significant insights into the grinding mechanism of particulate materials [49,50]. The digital twin modelling of nanoindentation is performed by atomistic simulation or molecular dynamics by many researchers [3,4,51].

As shown in Figure 12, the milling process spans a vast variety of characteristic length scales due to the fact that the multiscale information of particle breakage is inextricably linked. While the proposed multiscale modelling roadmap is appealing, the integration of information at all levels against a certain milling process is not always possible. There exists

a need to explore which scale of particle breakage information should be integrated and how to avoid excessive or overlapped information between the physical twin and digital twin. Furthermore, another general issue is how to opt in the appropriate modelling techniques in the multiscale context and what is the contribution of the opted computational model made in the milling process. Notably, this proposed conceptual framework can be well suited as a reference for developing multiscale strategy of other particulate processes alike such as granulation and fluidized bed drying.

Figure 12 Multiscale modelling roadmap with both physical twin and digital twin for particle breakage subject to milling events

5.2 Model validation

5.2.1 Digital platform and model validation cycle

At the heart of multiscale modelling approach is integrating the best available information across difference scales and defining a high-identity predictive model package embedding profound scientific process knowledge for a given milling operation. Various digital platforms have been developed by different research groups and commercial software suppliers, which can be used to implement the digital operation of the milling process using general programming languages or specialist platforms. In the present study, the digital platform of gPROMS Formulate Products is used for developing, customizing, and validating population balance model in the Dry Mill Module. The gPROMS environment has significant advantages of built-in mathematical equation solvers, graphical flowsheeting, parameter estimation and access to physical properties of many particulate materials [52].

Furthermore, the gPROMS platform has a strong capacity in data processing such as data import, data conversion and data loading which can easily access the numerical data from foreign software without a separate linking steps. Figure 13 presents a generic model validation cycle for input parameters estimation based on purposeful experimental data, comparative analysis between the computational and experimental output, and vastly extending the model predictive spectrum using global system analysis [52]. The model validation cycle can be divided as several connective steps [52]: (1) Generate a first-principle model corresponding to the experimentation process; (2) Perform initial experiments

including the first set of data for model calibration and second set of data for model validation; (3) Interrogate the model together with the first set of data to estimate model parameters of interest; (4) Run the model validation with the fitted parameters against the second set of data in step 2 ; (5) Ensure an acceptable level of mismatch and build the confidence in the model prediction; (6) In case of unacceptable level of discrimination between the model prediction and experiments, design further experiment to provide wide responsive space and refine the model definition or reselect some other fitted parameters to iterate steps 4 and 5; (7) Perform Global System Analysis on top of the validated model to explore the design space beyond the current experimental space.

Figure 13 Model validation cycle for process models (Modified from Spatenka et al. [52])

Note that this model validation cycle is generalized for advanced process modelling, which lends itself to a wide application of multiscale modeling of particulate processes including its application to the impact pin milling process herein.

5.2.2 Parameter estimation

The selection function and breakage function from Vogel and Peukert model are used for breakage kernels. There are total seven parameters in the Vogel and Peukert model and for simplicity a linear relationship between rotary speed and breakage rate is postulated. In calibrating the PBM, there are five empirical parameters in the breakage kernels using MAXLHD algorithm embraced in gPROMS [28]. The impact number and the specific energy are fixed constant as there is no correlation with the mechanical properties in the literature report. However, it is understandable that the average specific energy will increase with the growth of rotary speed. And the input values of specific energy are referred from our preceding publication of DEM modeling of particle dynamics under three rotary speeds 8000, 10000 and 12000 RPM [28]. Hence, there are three parameters to estimate in selection function and two parameters to estimate in breakage function. The fixed values and optimal values of these estimated parameters are summarized in Table 5 and Table 6. In particular, the relationship between the mechanical properties measured from the nanoscale and the material dependent parameters f_{mat} and $x * W_{m,min}$ is specified by the assignment of c_1 and c_2 following Eqs. 15a and 17a.

The fitted quality of PSD quantiles, d_{10}, d_{25}, d_{50}, d_{75} and d_{90} is depicted in Figure 14, which shows a mutually strong agreement between the fitted and measured values. The cumulative size distribution for the three rotary speeds is given in Figure 15.

Figure 14 Model calibration of PSD quantiles in 8000 RPM and 12000 RPM and validation in 10000 RPM

Figure 15 Model Validation with RPM 10000 RPM with calibrated parameters fitted from 8000 RPM and 12000 RPM

5.3 Global system analysis

A key feature of gPROMS digital platform is provision of Global System Analysis (GSA) to systematically explore the relative importance of model input parameters with regard to their influence on the model output responses. The GSA is becoming a prominent tool in design space extension and decision-making processes in particulate product manufacturing. The increasing demand of GSA is due to the complexity of particulate system and disability of enormous space exploration by experimental characterisation. The basic principle of GSA is based on drawing samples from the defined particulate system, i.e. extracting different values for individual parameter and calculating the corresponding responsive values. There are two types of GSA embedded in gPROMS, i.e. uncertainty analysis and sensitivity analysis. The uncertainty analysis is used to determine what effects of the input parameters have on the uncertainty in the system responses. This type of analysis can be achieved using the Monte Carlo method. The Monte Carlo method carries out multiple model evaluations with deterministic or probabilistic distribution and the responsive values of these evaluations are therefore used to interrogate the system uncertainty. The sensitivity analysis is used to determine which factor contributes most to the uncertainty in a response. The variance in the response can be resulted from the combination of three distinct elements: (1) the importance of the parameter (2) the range of the parameter (3) the variance of the parameter. Ideally, the uncertainty analysis precedes the sensitivity analysis and a sensitivity analysis without uncertainty analysis is usually illogical [53]. More details regarding the distinct differences between the uncertainty analysis and sensitivity analysis in Global

System Analysis can be found elsewhere [53,54]. In the present study, the uncertainty analysis on the basis of validated population balance model is carried out.

Before proceeding, the parameters in the validated population balance models need to be identified for a quantitative analysis of uncertainty. These parameters include the milling time, the kinetic energy $W_{m,kin}$, the material resistant parameters f_{Mat} and $x * W_{m,min}$, and the minimum breakage size y' in the breakage function. The reason for choosing these parameters is to cover the literally important parameters from the perspective of operational condition e.g. milling time, particle dynamics e.g. kinetic energy, particle intrinsic properties e.g. f_{Mat} , $x * W_{m,min}$ and y' respectively. The global system analysis of breakage rate and impact frequency can be found more details in our previous work [28]. The variance of the abovementioned parameters as well as their distribution mode is tabulated in Table 7.

The global system analysis of milling time on the cumulative size distribution is shown in Figure 16. It clearly shows a rapidly shifting trend to the left side in the first 10 seconds and the trend gradually slows down with minimal difference until 99 seconds. A specific zoom in the variation of d_{50} further confirms the initially significant role of milling time within 10 seconds. The value of d_{50} dramatically drops down from nearly 1200 μm to 21 μm at 9 seconds. Afterwards, the d_{50} decreases slightly and starts levelled off from 30 seconds to 99 seconds. This suggests a great potential to reduce the energy consumption by operating the impact pin mill with merely 30 seconds whilst maintaining almost the same fineness compared to the milling time at 90 seconds.

Figure 16 Global system analysis of milling time on the cumulative size distribution and d_{50} of zeolite particles under 10000 RPM rotary speed

Figure 17 demonstrates the effect of kinetic energy as a single variate with its influence on the cumulative size distribution. It shows that the kinetic energy has an increasingly large role in the coarse particle distribution. As the kinetic energy is increased from 500 J/Kg to 4900 J/Kg, the reduction ratio of d_{90} is way larger than that of d_{10}. The reduction of d_{50} falls between the reduction ratio of d_{90} and d_{10}. The d_{50} is shown to decrease in a hierarchal mode when the kinetic energy is gradually increased from 500 J/kg to 4900 J/kg. This

suggests the option of lower boundary value of kinetic energy instead of the upper boundary value to promote the energy efficiency for the sake of the same magnitude of size reduction ratio.

Figure 17 Global system analysis of kinetic energy $W_{m,kin}$ on the particle size distribution and d_{50}

In Figure 18, the effect of f_{mat} on the cumulative size distribution is shown negligible irrespective of the variation in the testing regime.

Figure 18 Global system analysis of f_{mat} on the particle size distribution and d_{50}

As the input value of f_{mat} almost covers the full spectrum sourced in the literature, this implies that f_{mat} will be least influential parameter subject to the high impact velocity and high impact frequency in the impact pin mill. This observation also applies to the influence on the variation of d_{50}. As a stark contrast in Figure 19, the global system analysis of another key material-dependent parameter $x * W_{min}$ shows a vastly different effect in the size distribution curve. The increased value of $x * W_{m,min}$ under the same kinetic energy results in the increase of threshold breakage size and a consequent increase of d_{50}. However, it is interesting to note that there are nine cumulative size distribution curves whereas the interval of variation is set as 50. This infers a leap forward shift of distribution curve where the distribution curve stays unchanged over a certain amount of intervals. This is evidenced by the depiction of d_{50} over the regime of $x * W_{min}$ between 0.02 and 2.5. The reason for this kind of variation is still under investigation but a clear take-away message is that $x * W_{min}$ is a much more prevailing parameter compared to f_{mat} in the Vogel and Peukert model [34].

Figure 19 Global system analysis of $x * W_{min}$ on the particle size distribution and d_{50}

Figure 20 indicates the shift of the size curve to right side when the value of minimum breakage size is varied from 1 μm to 49 μm. Interestingly, the effect of minimum breakage size is more pronounced in the finer particle size. This can be exemplified by the widening gap in the d_{10} compared to the narrow gap in the d_{90}. The d_{50} is witnessed to increase

sharply until 20 μm and then steadily increase with a slower pace until 49 μm. Figure 20 implies that the minimum breakage size will be a key parameter in a rigorous control of the finer particles.

Figure 20 Global system analysis of minimum breakage size y' on the particle size distribution and d_{50}

6   Conclusions

This paper has presented a comprehensive study to tackle the challenge in interlinking the information of particle breakage from distinctively different scales. A hybrid model of theoretical, experimental and numerical attempts for particle breakage was conducted through nanoindentation test, milling tests and population balance model accordingly. The reason of performing nanoindentation tests is because particle reaction to the applied stresses depends on their inherent mechanical properties [2]. The impact milling tests through an impact pin mill shed insights into the effect of rotary speed in milling performance. The appropriate definition of the selection function and the breakage function in the population balance model is rooted in the prevailing mechanism of fragmentation subject to high impact velocity. With the aid of collective data from the impact pin mill, the population balance model is first calibrated in the rotary speed of 8000 RPM and 12000 RPM whilst the model validation is carried out with the rotary speed of 10000 RPM.

A conceptual multiscale modelling roadmap for particle breakage in milling is proposed to integrate the most useful and best available information across different scales. In particular, the complementary strength of physical twin and digital twin can be paired to overcome the drawbacks in the counterpart across each scale in the proposed roadmap. Global system analysis is also carried out to vastly extend the predictive capacity in a virtually trustworthy environment. In contrary to exhausting the information at single scale, the uniqueness of the multiscale modelling proposal is to extract the most valuable pieces of data in the available scales and thus form all the deterministic information in PBM. A systematic consideration of milling process via a multiscale modelling approach is shown to be capable of transitioning the intensively inefficient and energy-consuming milling into digital operation with efficiency. Digital twin can be used to substantially reduce expenditure and

energy consumption whilst maintaining its accuracy and fidelity. A generic modelling platform to couple the milling dynamics into the milling evolution with digital maturity will be highly desirable to facilitate the milling efficacy and substantially reduce the environmental footprint.

Acknowledgement

Credit Author Statement

Dear Editors

I can confirm that the contributions of co-authors in making this manuscript are presented as below:

Li Ge Wang: Writing-Original Draft, Methodology, Software

Ruihuan Ge: Data curation, Formal analysis, Resources

Xizhong Chen: Conceptualization, Supervision, Writing-Reviewing and Editing

Rongxin Zhou: Software, Validation, Writing-Reviewing and Editing

Han-Mei Chen: Visualization, Investigation

This statement has been fully agreed by the abovementioned authors.

Yours Sincerely

Xizhong Chen

Lecturer in Particulate Process Modelling

Process and Chemical Engineering, University College Cork, Ireland

Email: Xizhong.Chen@ucc.ie

Conflict of interest: None

References

[1]   G.D. Ingram, I.T. Cameron, Challenges in multiscale modelling and its application to granulation systems, Dev. Chem. Eng. Miner. Process. 12 (2004) 293–308. doi:10.1002/apj.5500120408.

[2]   W. Peukert, Material properties in fine grinding, Int. J. Miner. Process. 74 (2004) 3–17. doi:10.1016/j.minpro.2004.08.006.

[3]   T.H. Fang, J.H. Wu, Molecular dynamics simulations on nanoindentation mechanisms of multilayered films, Comput. Mater. Sci. 43 (2008) 785–790. doi:10.1016/j.commatsci.2008.01.066.

[4]   U. Landman, W.D. Luedtke, N.A. Burnham, R.J. Colton, Atomistic mechanisms and dynamics of adhesion, nanoindentation, and fracture, Science (80-.). 248 (1990) 454–461. doi:10.1126/science.248.4954.454.

[5]   S.Z. Chavoshi, S. Xu, Nanoindentation/scratching at finite temperatures: Insights from atomistic-based modeling, Prog. Mater. Sci. 100 (2019) 1–20. doi:10.1016/j.pmatsci.2018.09.002.

[6]   L. Sikong, H. Hashimoto, S. Yashima, Breakage behavior of fine particles of brittle minerals and coals, Powder Technol. 61 (1990) 51–57. doi:10.1016/0032-5910(90)80065-7.

[7]   P.H. Shipway, I.M. Hutchings, Attrition of brittle spheres by fracture under compression and impact loading, Powder Technol. 76 (1993) 23–30. doi:10.1016/0032-5910(93)80037-B.

[8]   K. Danjo, H. Kato, A. Otsuka, K. Ushimaru, Fundamental study on the evaluation of strength of granular particles, Chem. Pharm. Bull. 42 (1994) 2598–2603. doi:10.1248/cpb.37.3229.

[9]   B. Van Veen, Compaction of Powder Blends Effect of pores, particles and percolation on tablet strength, 2003. http://dissertations.ub.rug.nl/faculties/science/2003/b.van.veen/?pLanguage=en&pFullItemRecord=ON.

[10]   Y. Petukhov, H. Kalman, A new apparatus for particle impact tests, Part. Part. Syst. Charact. 20 (2003) 267–275. doi:10.1002/ppsc.200390032.

[11]   L. Vogel, W. Peukert, Determination of material properties relevant to grinding by practicable labscale milling tests, Int. J. Miner. Process. 74 (2004) 329–338. doi:10.1016/j.minpro.2004.07.018.

[12]   L. Vogel, W. Peukert, From single particle impact behaviour to modelling of impact mills, Chem. Eng. Sci. 60 (2005) 5164–5176. doi:10.1016/j.ces.2005.03.064.

[13]   W.C. Oliver, G.M. Pharr, Measurement of hardness and elastic modulus by instrumented indentation: Advances in understanding and refinements to methodology, J. Mater. Res. 19 (2004) 3–20. doi:10.1557/jmr.2004.19.1.3.

[14]   A.G. Evans, T.R. Wilshaw, Quasi-static solid particle damage in brittle solids -- I. Observations, analysis and implications, Acta Metall. 24 (1976) 939–956. doi:doi.org/10.1016/0001-6160(76)90042-0.

[15]   A.G. Evans, M.E. Gulden, M. Rosenblatt, Impact Damage in Brittle Materials in the Elastic-Plastic Response Regime, Proc. R. Soc. A Math. Phys. Eng. Sci. 361 (1978) 343–365. doi:10.1098/rspa.1978.0106.

[16] W.C. Oliver, G.M. Pharr, An improved technique for determining hardness and elastic modulus using load and displacement sensing indentation experiments, Mater. Res. Soc. 7 (1992) 1992.

[17] L.G. Wang, Z.P. Li, L.Z. Zhang, R.X. Zhou, X.Z. Chen, On the Measurement of Particle Contact Curvature and Young's Modulus Using X-ray μCT, Appl. Sci. 11 (2021).

[18] G.R. Anstis, P. Chantikul, B.R. Lawn, D.B. Marshall, A critical evaluation of indentation techniques for measuring fracture toughness: I, Direct crack measurements, 46 (1981) 533–538. doi:10.1111/j.1151-2916.1981.tb10320.x.

[19] M. Marigo, D.L. Cairns, J. Bowen, A. Ingram, E.H. Stitt, Relationship between single and bulk mechanical properties for zeolite ZSM5 spray-dried particles, Particuology. 14 (2014) 130–138. doi:10.1016/j.partic.2013.05.006.

[20] L.J. Taylor, D.G. Papadopoulos, P.J. Dunn, a. C. Bentham, N.J. Dawson, J.C. Mitchell, M.J. Snowden, Predictive milling of pharmaceutical materials using nanoindentation of single crystals, Org. Process Res. Dev. 8 (2004) 674–679. doi:10.1021/op0300241.

[21] L.J. Taylor, D.G. Papadopoulos, P.J. Dunn, A.C. Bentham, J.C. Mitchell, M.J. Snowden, Mechanical characterisation of powders using nanoindentation, Powder Technol. 143–144 (2004) 179–185. doi:10.1016/j.powtec.2004.04.012.

[22] M. Meier, E. John, D. Wieckhusen, W. Wirth, W. Peukert, Influence of mechanical properties on impact fracture: Prediction of the milling behaviour of pharmaceutical powders by nanoindentation, Powder Technol. 188 (2009) 301–313. doi: 10.1016/j.powtec.2008.05.009.

[23] C. Hare, L. Wang, J.Y. Ooi, Characterisation of Particle Grindability by Indentation and Impact, International Fine Particle Research Institute, 2015.

[24] L.G. Wang, Particle Breakage Mechanics in Milling Operation, University of Edinburgh, 2016.

[25] B.R. Lawn, D.B. Marshall, Hardness, toughness and brittleness, an indentation analysis, J. Am. Ceram. Soc. 62 (1979) 347–350.

[26] J. Litster, Chapter 5, Particle Size Reduction, Design and Processing of Particulate Products, Cambridge University Press, 2016.

[27]   A. El Hagrasy, L.G. Wang, J. Litster, Continuous Wet Granulation, in: Z. Nagy, A. Hagrasy, Litster JD (Eds.), Contin. Pharm. Process., Springer, 2020.

[28]   Z.P. Li, L.G. Wang, W. Chen, X. Chen, C. Liu, D. Yang, Scale-up Procedure of Parameter Estimation in Selection and Breakage Functions for Impact Pin Milling, Adv. Powder Technol. (2020).

[29]   C. Labra, J.Y. Ooi, J.F. Chen, J. Sun, Numerical analysis of impact events in a centrifugal impact pin mill, AIP Conf. Proc. 1542 (2013) 935–938. doi:10.1063/1.4812086.

[30]   H. Kalman, V. Rodnianski, M. Haim, A new method to implement comminution functions into DEM simulation of a size reduction system due to particle-wall collisions, Granul. Matter. 11 (2009) 253–266. doi:10.1007/s10035-009-0140-8.

[31]   H. Rumpf, Physical aspects of comminution and new formulation of a law of comminution, Powder Technol. 7 (1973) 145–159. doi:10.1016/0032-5910(73)80021-X.

[32]   R. Weichert, Theoretical Prediction of Energy Consumption and Particle Size Distribution in grinding and drilling of brittle materials, Part. Part. Syst. Charact. (1991).

[33]   H. Hertz, Über die Berührung fester elastischer Körper., J. Für Die Reine Und Angew. Math. (1881) 156–171.

[34]   L. Vogel, W. Peukert, Breakage behaviour of different materials - Construction of a mastercurve for the breakage probability, Powder Technol. 129 (2003) 101–110. doi:10.1016/S0032-5910(02)00217-6.

[35]   M. Meier, E. John, D. Wieckhusen, W. Wirth, W. Peukert, Characterization of the grinding behaviour in a single particle impact device: studies on pharmaceutical powders., Eur. J. Pharm. Sci. 34 (2008) 45–55. doi:10.1016/j.ejps.2008.02.120.

[36]   F. Shi, T. Kojovic, Validation of a model for impact breakage incorporating particle size effect, Int. J. Miner. Process. 82 (2007) 156–163. doi:10.1016/j.minpro.2006.09.006.

[37]   O. Lecoq, A. Chamayou, J.A. Dodds, P. Guigon, Application of a simplifying model to the breakage of different materials in an air jet mill, Int. J. Miner. Process. 112–113 (2012) 7–12. doi:10.1016/j.minpro.2012.04.004.

[38]   F. Lyu, M. Thomas, W.H. Hendriks, A.F.B. van der Poel, Size reduction in feed technology and methods for determining, expressing and predicting particle size: A review, Anim. Feed Sci. Technol. 261 (2020) 114347. doi:10.1016/j.anifeedsci.2019.114347.

[39]   H. Richard, Crushing and classification, in: Fundam. Part. Technol., 2002.

[40]   S.R. Broadbent, T.G. Callcott, A matrix analysis of process involving particle assemblies, Philos. Trans. R. Soc. London. Ser. A, Math. Phys. Sci. 249 (1956) 99–123.

[41]   G.M. Campbell, C. Webb, On Predicting Roller Performance Part vI: the breakage equation, (2001) 234–242.

[42]   M.H. Wang, R.Y. Yang, A.B. Yu, DEM investigation of energy distribution and particle breakage in tumbling ball mills, Powder Technol. 223 (2012) 83–91. doi:10.1016/j.powtec.2011.07.024.

[43]   B. Olaleye, F. Pozza, C.Y. Wu, L.X. Liu, Population balance modelling of ribbon milling with a new mass-based breakage function, Int. J. Pharm. 571 (2019) 118765. doi:10.1016/j.ijpharm.2019.118765.

[44]   L. Simone, C.Y. Wu, G. Reynolds, M. Andreja, S. Jonathan, DEM–PBM Modeling of Impact Dominated Ribbon Milling, AIChE J. 63 (2017) 3692–3705. doi:10.1002/aic.

[45]   B. Zhao, J. Wang, G. Coop, M.R.; Viggiani, J. M, An investigation of single sand particle fracture using X-ray micro-tomography, Géotechnique. 65 (2015) 625–641. doi:10.1680/geot.14.P.157.

[46]   R. Ge, M. Ghadiri, T. Bonakdar, Q. Zheng, Z. Zhou, I. Larson, K. Hapgood, Deformation of 3D printed agglomerates: Multiscale experimental tests and DEM simulation, Chem. Eng. Sci. 217 (2020) 115526. doi:10.1016/j.ces.2020.115526.

[47]   R. Ge, L. Wang, Z. Zhou, DEM analysis of compression breakage of 3D printed agglomerates with different structures, Powder Technol. 356 (2019) 1045–1058. doi:10.1016/j.powtec.2019.08.113.

[48]   R. Ge, M. Ghadiri, T. Bonakdar, K. Hapgood, 3D printed agglomerates for granule breakage tests, Powder Technol. 306 (2017) 103–112. doi:10.1016/j.powtec.2016.10.070.

[49]   S. Malkin, T.W. Hwang, Grinding mechanisms for ceramics, CIRP Ann. Technol. 45
        (1996) 569–580. doi:10.1016/S0007-8506(07)60511-3.

[50]   M. Meier, E. John, D. Wieckhusen, W. Wirth, W. Peukert, Generally applicable
        breakage functions derived from single particle comminution data, Powder Technol.
        194 (2009) 33–41. doi:10.1016/j.powtec.2009.03.018.

[51]   O. Tsoungui, D. Vallet, J.C. Charmet, Numerical model of crushing of grains inside
        two-dimensional granular materials, Powder Technol. 105 (1999) 190–198.
        doi:10.1016/S0032-5910(99)00137-0.

[52]   S. Spatenka, M. Matzopoulos, Z. Urban, A. Cano, From Laboratory to Industrial
        Operation: Model-Based Digital Design and Optimization of Fixed-Bed Catalytic
        Reactors, Ind. Eng. Chem. Res. 58 (2019) 12571–12585. doi:10.1021/acs.iecr.9b01314.

[53]   A. Saltelli, K. Aleksankina, W. Becker, P. Fennell, F. Ferretti, N. Holst, S. Li, Q. Wu, Why
        so many published sensitivity analyses are false: A systematic review of sensitivity
        analysis practices, Environ. Model. Softw. 114 (2019) 29–39.
        doi:10.1016/j.envsoft.2019.01.012.

[54]   S. Kucherenko, B. Feil, N. Shah, W. Mauntz, The identification of model effective
        dimensions using global sensitivity analysis, Reliab. Eng. Syst. Saf. 96 (2011) 440–449.
        doi:10.1016/j.ress.2010.11.003.

Table 1 Measured hardness and Young's modulus of zeolite particles by indentation

Zeolite Particle 1.4-1.7 mm	Hardness (GPa)	Young's modulus (GPa)
1	0.15	6.38
2	0.24	6.19
3	0.18	5.92
4	0.15	4.89
5	0.21	6.89

6	0.21	6.72
7	0.18	6.35
8	0.13	5.74
9	0.19	6.39
10	0.29	7.74
Average	0.19	6.32
Standard deviation	0.045	0.75
Coefficient of Variation	0.24	0.12

Table 2 Summarized fracture toughness values measured from Nano-indentation

Fracture toughness	Zeolite (1.4-1.7 mm)
Average $(MPa.m^{1/2})$	0.13
Standard Deviation $(MPa.m^{1/2})$	0.07
Coefficient Variation	0.54

Table 3 Pin configuration in the impact pin mill UPZ100

Rotary disc	Ring radius (mm)	Pin No.	Pin spacing (mm)	Pin radius (mm)	Net spacing (mm)
R1	31	24	8.11	1.5	5.11
S2	35	32	6.87	1.5	3.87
R3	39	40	6.12	1.5	3.12
S4	43	44	6.14	1.5	3.14

R5	47	58	5.09	1.5	2.09
S6	51	54	5.93	1.5	2.93
R7	55	70	4.93	1.5	1.93
S8	59	62	5.98	1.5	2.98

Table 4 PSD quantiles of zeolite particles (1.2-2.0 mm) at varying rotary speed

Rotary speed (RPM)	d_n (μm)				
	d_{10}	d_{25}	d_{50}	d_{75}	d_{90}
8000	2.45	7.21	42.38	97.49	169.66
10000	2.01	4.63	10.84	47.53	85.91
12000	1.78	3.17	7.32	25.21	55.53

Table 5 Input parameters with fixed constants in the population balance model

Category	Input parameter	Initial value			Multiscale
Selection function	Impact number, k	350			Particle scale
	Specific energy, $W_{m,kin}$ (J/kg)	8000 RPM	10000 RPM	12000 RPM	Particle scale
		1250	2450	2800	

Table 6 Input parameters to estimate in the population balance model

Category	Input parameter	Initial value	Optimal value	Multiscale category

Category	Parameters			Scale
Selection function	S_x (/s)	0.1	0.524	Particle scale
	c_1 (f_{mat})	0.0348 (0.464)	0.0446 (0.596)	Nano scale
	c_2 ($x * W_{m,min}$)	0.03 (0.10)	0.0723 (0.24)	Nano scale
Breakage function	q	0.28	0.37	Particle scale
	y' (μm)	2.55	1.95	Particle scale

Table 7 Summary of parameters variance and distribution mode for uncertainty analysis

Category	Parameters	Lower bound	Upper bound	Number of intervals
Selection function	milling time, (s)	1	99	
	Kinetic energy, $W_{r,k,min}$ (J/Kg)	500	4900	
	f_{mat} (kg/Jm)	0.1	3.04	
	$x * W_{min}$ (Jm/Kg)	0.02	2.45	50
Breakage function	y', Minimum breakage size (μm)	2	50	
Operational condition	Milling time (s)	10	250	

Graphical abstract

Highlights

- A multiscale digital twin for particle breakage in milling is presented.

- Mechanistic link from nanoindentation to population balance model is developed.

- A conceptual modelling roadmap to integrate multiscale information is proposed.

- Impact pin mill tests are carried out to provide dataset for model validation.
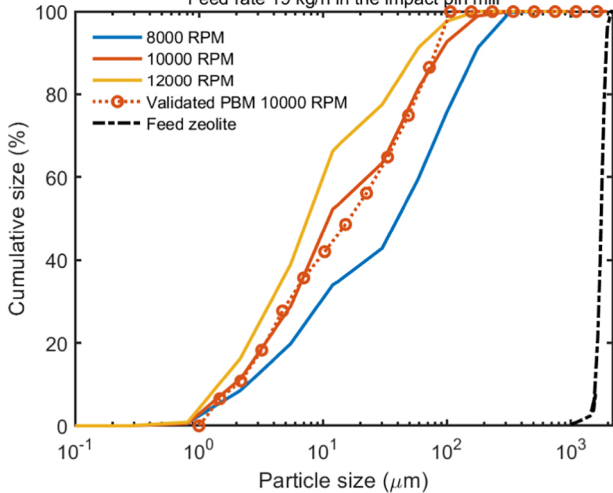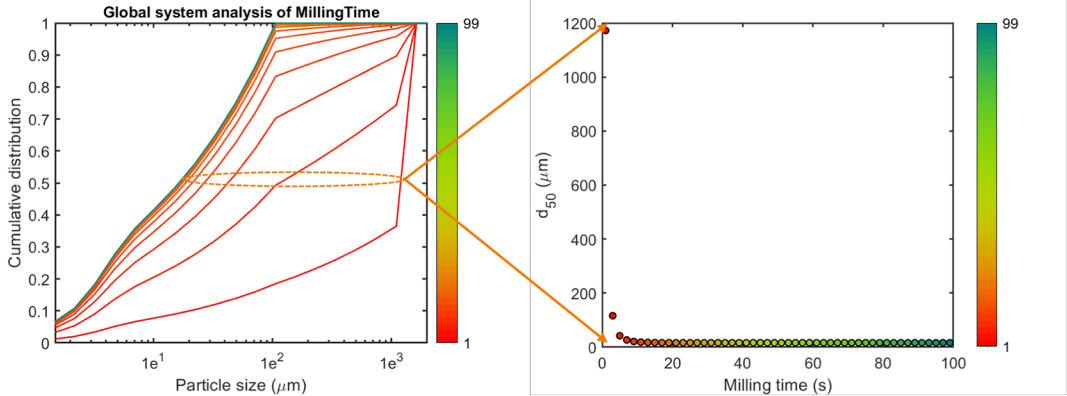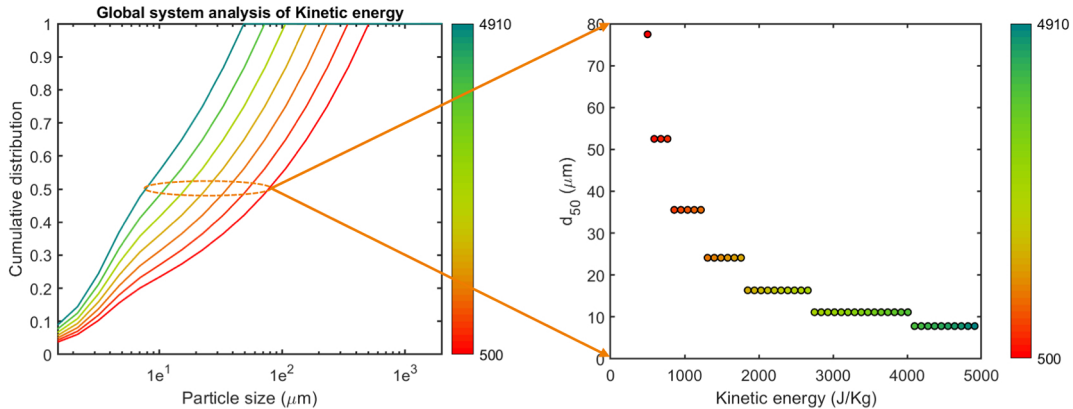
- Global system analysis of validated population balance model is performed.
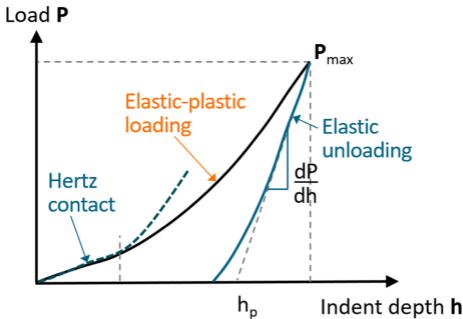
Figure 1
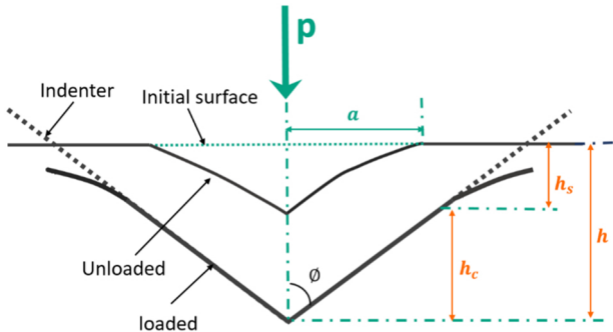
Figure 2
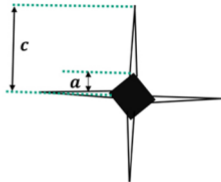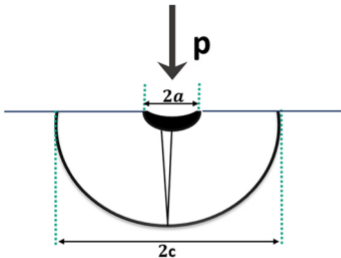
Figure 3
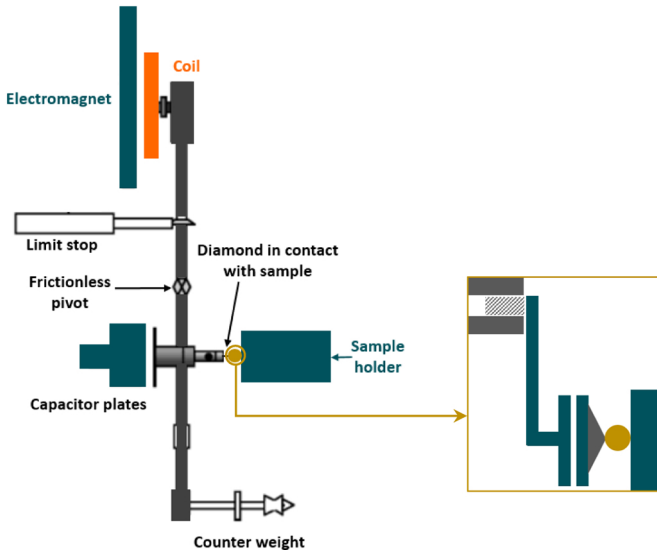
Figure 4
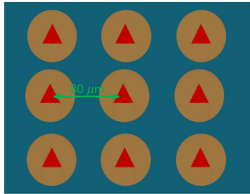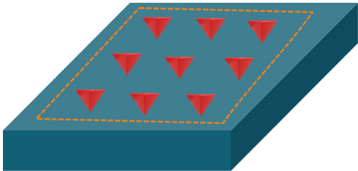
Figure 5
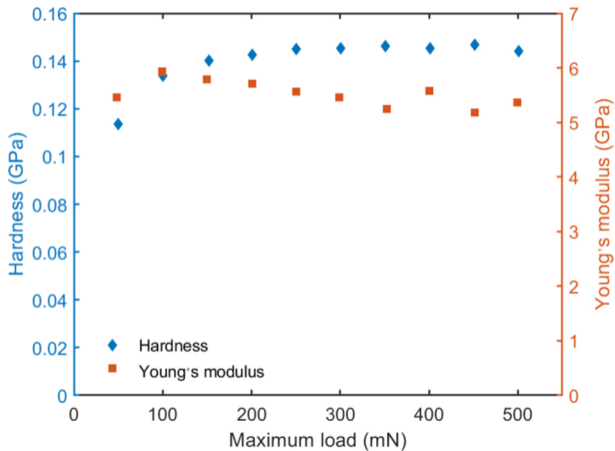
Figure 6

Figure 7

Figure 8

Particles feed inlet

Stationary plate

Rotary plate

Outlet
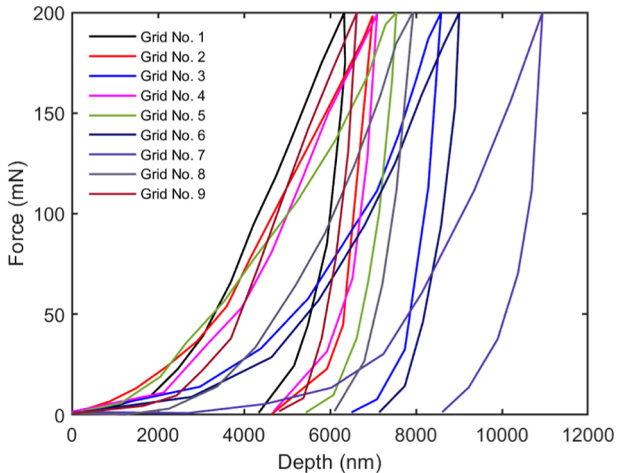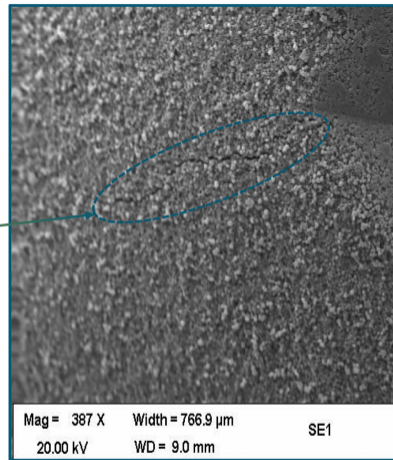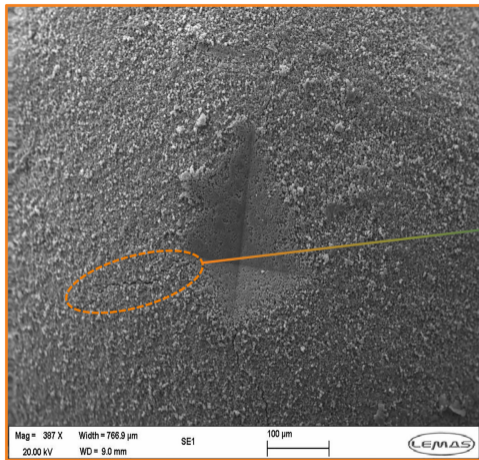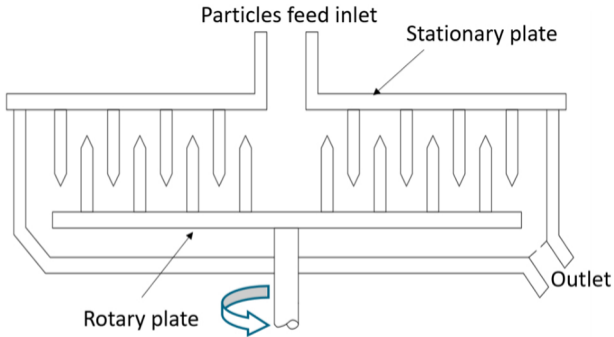
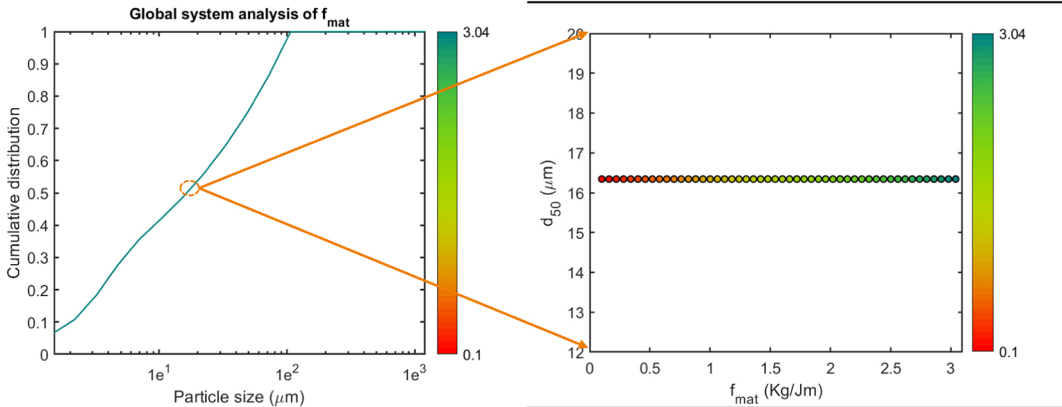Figure 9

Figure 10

Figure 11
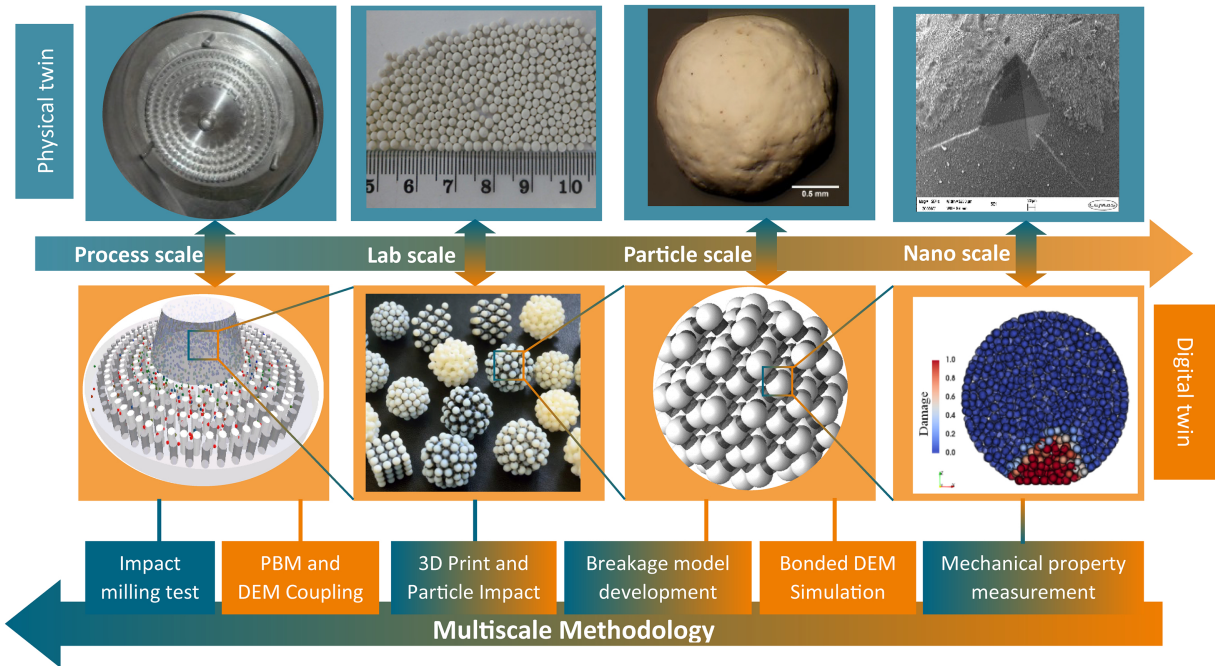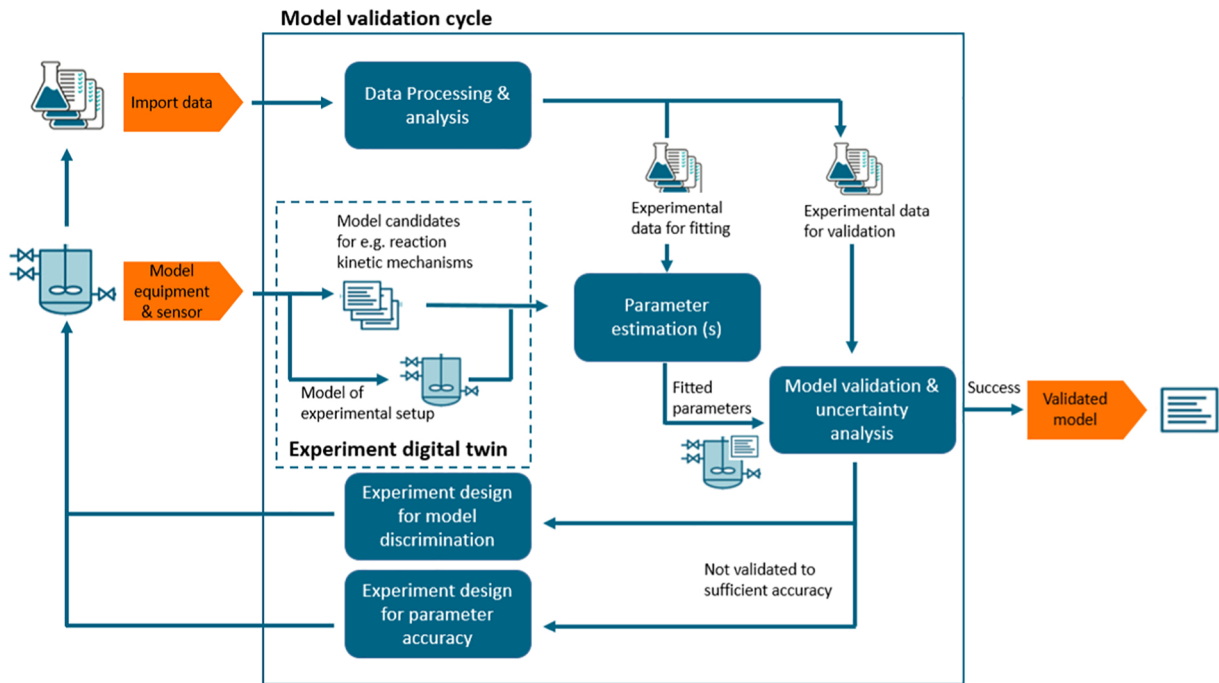
Figure 12

Figure 13
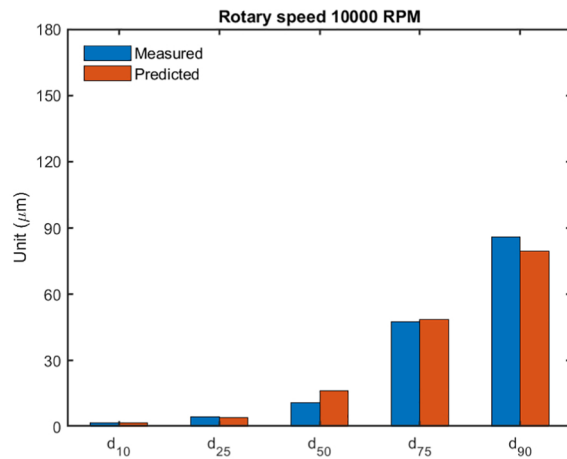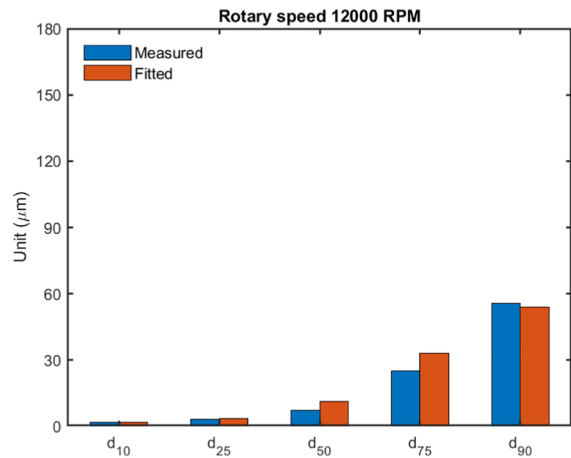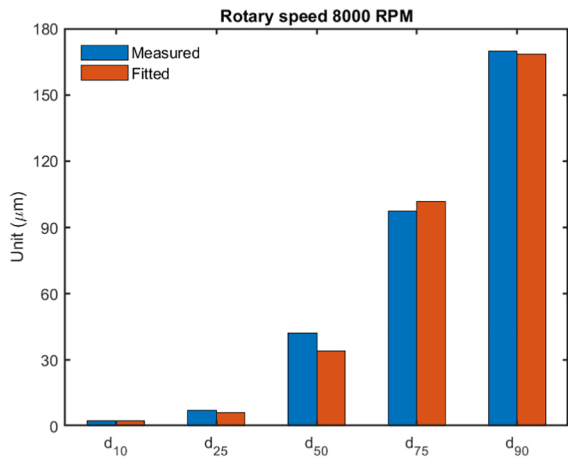
Figure 14

Figure 15

Figure 16

Figure 17

Figure 18

Figure 19

Figure 20